excitations appear. The scaling laws predicted by ERMT are compatible with the numerical results that we have obtained for the soft-sphere model. This approach is equivalent to other microscopic descriptions of the glass transition based on the geometry of the PEL[5–7,31]. But this point of view emphasizes quantities accessible to experiment, like the VDOS, and proposes an interpretation of a universal feature of glasses, the boson peak. This peak appears in the phonon phase, and it is a signature of a cross-over from a phonon-dominated spectrum with a Debye ω^2 scaling to an ω^γ, $\gamma \approx 1.5$ spectrum, resulting from the hybridization of acoustic modes with high-energy modes that soften upon approaching the saddle–phonon transition[9]. The ERMT predictions (equations (1) and (2)) could be checked experimentally in hyperquenching experiments, where the boson peak should strongly depend on the fictive temperature. We expect that the 'saddle–phonon transition' point of view will be able to bridge the realms of experiment and numerical studies of the PEL, allowing the testing of many geometrical ideas, and the use of insights derived from PEL in the detailed analysis of the experimental glass transition. □

Received 10 July 2002; accepted 30 January 2003; doi:10.1038/nature01475.

1. Angell, C. A. Formation of glasses from liquids and biopolymers. *Science* **267,** 1924–1935 (1995).
2. DeBenedetti, P. G. & Stillinger, F. H. Supercooled liquids and the glass transition. *Nature* **410,** 259–267 (2001).
3. Sette, F., Krisch, M. H., Masciovecchio, C., Ruocco, G. & Monaco, G. Dynamics of glasses and glass-forming liquids studied by inelastic X-ray scattering. *Science* **280,** 1550–1555 (1998).
4. Stillinger, F. H. A topographic view of supercooled liquids and glass formation. *Science* **267,** 1935–1939 (1995).
5. Angelani, L., Di Leonardo, R., Ruocco, G., Scala, A. & Sciortino, F. Saddles in the energy landscape probed by supercooled liquids. *Phys. Rev. Lett.* **85,** 5356–5359 (2000).
6. Broderix, K., Bhattacharya, K. K., Cavagna, A., Zippelius, A. & Giardina, I. Energy landscape of a Lennard-Jones liquid: Statistics of stationary points. *Phys. Rev. Lett.* **85,** 5360–5363 (2000).
7. Grigera, T. S., Cavagna, A., Giardina, I. & Parisi, G. Geometric approach to the dynamic glass transition. *Phys. Rev. Lett.* **88,** 055502 (2002).
8. Mézard, M., Parisi, G. & Zee, A. Spectra of euclidean random matrices. *Nucl. Phys. B* **559,** 689–701 (1999).
9. Grigera, T. S., Martín-Mayor, V., Parisi, G. & Verrocchio, P. Vibrations in glasses and Euclidean random matrix theory. *J. Phys. Condens. Matter* **14,** 2167–2179 (2002).
10. Phillips, W. A., Buchenau, U., Nücher, N., Dianoux, A.-J. & Petry, W. Dynamics of glassy and liquid selenium. *Phys. Rev. Lett.* **63,** 2381–2384 (1989).
11. Ruocco, G. *et al.* Relaxation processes in harmonic glasses? *Phys. Rev. Lett.* **84,** 5788–5791 (2000).
12. Pilla, O. *et al.* Transverse acoustic nature of the excess of vibrational states in vitreous silica. Preprint cond-mat/0209519 at ⟨http://xxx.lanl.gov⟩ (2002).
13. Masciovecchio, C. *et al.* Observation of large-momentum phononlike modes in glasses. *Phys. Rev. Lett.* **76,** 3356–3359 (1996).
14. Matic, A. *et al.* Contrasting behaviour of acoustic modes in network and non-network glasses. *Europhys. Lett.* **54,** 77–83 (2001).
15. Masciovecchio, C. *et al.* High-frequency propagating modes in vitreous silica at 295 K. *Phys. Rev. B* **55,** 8049–8051 (1997).
16. Benassi, P. *et al.* Evidence of high frequency propagating modes in vitreous silica. *Phys. Rev. Lett.* **77,** 3835–3838 (1996).
17. Fioretto, D. *et al.* High-frequency dynamics of glass-forming polybutadiene. *Phys. Rev. E* **59,** 4470–4475 (1999).
18. Pilla, O. *et al.* Nature of the short wavelength excitations in vitreous silica: An X-ray Brillouin scattering study. *Phys. Rev. Lett.* **85,** 2136–2139 (2000).
19. Martín-Mayor, V., Mézard, M., Parisi, G. & Verrocchio, P. The dynamical structure factor in topologically disordered systems. *J. Chem. Phys.* **114,** 8068–8081 (2001).
20. Grigera, T. S., Martín-Mayor, V., Parisi, G. & Verrocchio, P. Vibrational spectrum of topologically disordered systems. *Phys. Rev. Lett.* **87,** 085502 (2001).
21. Götze, W. & Sjorgen, L. Relaxation processes in supercooled liquids. *Rep. Prog. Phys.* **55,** 241–376 (1992).
22. Kob, W. & Andersen, H. C. Testing mode-coupling theory for a supercooled binary Lennard-Jones mixture I: The van Hove correlation function. *Phys. Rev. E* **51,** 4626–6241 (1995).
23. Göetze, W. & Mayr, M. Evolution of vibrational excitations in glassy systems. *Phys. Rev. E* **61,** 587–606 (2000).
24. Cavagna, A., Giardina, I. & Parisi, G. Role of saddles in mean-field dynamics above the glass transition. *J. Phys. A* **34,** 5317–5326 (2001).
25. Bernu, B., Hansen, J.-P., Hiwatari, Y. & Pastore, G. Soft-sphere model for the glass transition in binary alloys: Pair structure and self-diffusion. *Phys. Rev. A* **36,** 4891–4903 (1987).
26. Grigera, T. S. & Parisi, G. Fast Monte Carlo algorithm for supercooled soft spheres. *Phys. Rev. E* **63,** 045102 (2001).
27. Kob, W., Sciortino, F. & Tartaglia, P. Aging as dynamics in configuration space. *Europhys. Lett.* **49,** 590–596 (2000).
28. Engberg, D. *et al.* Origin of the boson peak in a network glass B_2O_3. *Phys. Rev. B* **59,** 4053–4057 (1999).
29. Mamedov, S., Kisliuk, A. & Quitmann, D. Effect of preparation conditions on the low frequency Raman spectrum of glassy As_2S_3. *J. Mater. Sci.* **33,** 41–43 (1998).
30. Horbach, J., Kob, W. & Binder, K. The specific heat of amorphous silica within the harmonic approximation. *J. Phys. Chem. B* **103,** 4104–4108 (1999).
31. La Nave, E., Stanley, H. E. & Sciortino, F. Configuration space connectivity across the fragile-to-strong transition in silica. *Phys. Rev. Lett.* **88,** 035501 (2002).

Acknowledgements We thank O. Pilla, G. Ruocco and G. Viliani for discussions. We are grateful to the RTN3 collaboration for CPU time in their cluster. V.M.M. was supported in part by the European Commission and the Spanish OCYT.

Competing interests statement The authors declare that they have no competing financial interests.

Correspondence and requests for materials should be addressed to V.M.-M. (e-mail: victor.martin@roma1.infn.it).

Detection of human influence on sea-level pressure

Nathan P. Gillett*, Francis W. Zwiers†, Andrew J. Weaver* & Peter A. Stott‡

** School of Earth and Ocean Sciences, University of Victoria, PO Box 3055, Victoria, British Columbia, V8W 3P6, Canada*
† Canadian Centre for Climate Modelling and Analysis, Meteorological Service of Canada, PO Box 1700, STN CSC, Victoria, British Columbia, V8W 2Y2, Canada
‡ Hadley Centre for Climate Prediction and Research, Met Office, Bracknell, Berkshire RG12 2SY, UK

Greenhouse gases and tropospheric sulphate aerosols—the main human influences on climate—have been shown to have had a detectable effect on surface air temperature[1–3], the temperature of the free troposphere and stratosphere[2,4] and ocean temperature[5,6]. Nevertheless, the question remains as to whether human influence is detectable in any variable other than temperature. Here we detect an influence of anthropogenic greenhouse gases and sulphate aerosols in observations of winter sea-level pressure (December to February), using combined simulations from four climate models. We find increases in sea-level pressure over the subtropical North Atlantic Ocean, southern Europe and North Africa, and decreases in the polar regions and the North Pacific Ocean, in response to human influence. Our analysis also indicates that the climate models substantially underestimate the magnitude of the sea-level pressure response. This discrepancy suggests that the upward trend in the North Atlantic Oscillation index[7] (corresponding to strengthened westerlies in the North Atlantic region), as simulated in a number of global warming scenarios[8–10], may be too small, leading to an underestimation of the impacts of anthropogenic climate change on European climate.

We use gridded observations of decadal mean December–February sea-level pressure (1948–1998) taken from three sources: a version of the HadSLP data set derived using only surface observations[11], the National Centers for Environmental Prediction (NCEP) reanalysis[12], and an updated version of the Trenberth data set[13]. Intercomparison of these data sets indicates that agreement is generally good over those regions covered by observations, and that the Trenberth data and NCEP reanalysis differ mainly over Greenland and the Himalayas, probably owing to differences in the reduction of surface pressure to sea level. In regions where there are few surface observations, such as the Antarctic, the NCEP reanalysis is likely to be less reliable than in the better-sampled regions covered by all three data sets. We use ensembles of integrations with historical greenhouse gas and sulphate aerosol forcing from four coupled ocean–atmosphere climate models: the first and second Canadian Centre for Climate Modelling and Analysis coupled models, CGCM1 and CGCM2, and the second and third Hadley Centre coupled models, HadCM2 and HadCM3.

Figure 1 shows the trend in sea-level pressure over the 1948–1998 period in the NCEP reanalysis (Fig. 1a) and the multi-model mean

response (a mean over all available ensemble members) (Fig. 1b). The most notable features of the observed trend are decreases in sea-level pressure over the Arctic, Antarctic and North Pacific, and an increase over the subtropical North Atlantic, southern Europe and North Africa. These features were found to be significant compared to simulated internal variability, and are reproduced in response to greenhouse gas and sulphate aerosol forcing in all four models, and thus also in the multi-model mean (Fig. 1b). The amplitude of the simulated trends is, however, much less than that observed. Some authors have suggested that such a discrepancy might result from deficiencies in the modelled response to sea surface temperature variations[14], or a lack of stratospheric resolution[8], but such suggestions are controversial, and this issue remains open to debate[15]. The difference in simulated and observed trends over the Antarctic is partly attributable to stratospheric ozone depletion: simulated sea-level pressure changes in integrations of HadCM3 that also included stratospheric ozone changes were larger over the Antarctic, but agreed no better with observations over the Northern Hemisphere. The inclusion of solar and volcanic changes also did not resolve this discrepancy.

Until now, model simulations and observations of sea-level pressure changes have only been compared using indices such as the North Atlantic Oscillation index[10]. Here we apply an optimal detection approach to gridded sea-level pressure fields, thereby using more spatio-temporal information to assess whether the observed changes are likely to have been due to natural variability, and if not, whether they are consistent with those simulated in response to anthropogenic forcing.

The optimal detection approach[3] assumes that the observations (**y**) may be represented as the linear sum of the scaled simulated response to greenhouse gases and sulphate aerosol (**x**), and natural variability (**u**):

$$\mathbf{y} = \beta\mathbf{x} + \mathbf{u}$$

We apply signal-to-noise optimization, and account for uncertainty in the modelled response pattern by estimating β, the regression coefficient, with a total least-squares fit[3]. Owing to the limited length of control integration available, we reduce the number of degrees of freedom of our detection vector by regridding to a coarse grid (60° × 25°), and truncating onto the first ten empirical orthogonal functions (EOFs) of control variability[3].

We check whether this model provides a plausible explanation of the observations by testing whether the residual, **u**, is consistent with control variability at the 5% level[16]. The uncertainty in β is then assessed from control variability, and the forcing response pattern is detected if β is found to be inconsistent with zero. Averaging results from multiple models has been found to improve estimates of the long-term mean[17] and seasonal forecasts[18] of atmospheric variables, as well as estimates of the surface temperature response to anthropogenic forcing[19]. Thus, in order to increase the signal-to-noise ratio and reduce the effect of individual model errors, we use data from all four models simultaneously in the analysis, taking a mean of the simulated responses, and using concatenated control integrations from all four models to estimate internal variability[19].

Figure 2 shows the regression coefficient, β, estimated using this multi-model mean response pattern and each of the three observational data sets. It is significantly greater than zero in each case, indicating that an anthropogenic response is detected. The residual, **u**, was also found to be consistent with control variability in each case. However, based on 1948–1998 data, the associated 5–95% uncertainty ranges on β do not include unity in any case. This suggests that the models significantly underestimate the amplitude of the sea-level pressure response to greenhouse gas and sulphate aerosol increases, assuming there is no systematic overestimate of the changes in all three observed data sets. This result is consistent with the relative amplitudes of the responses shown in Fig. 1, and was found to be robust to variations in the EOF truncation between 6 and 30, and the use of an ordinary least-squares regression, rather than a total least-squares regression. We also obtained similar results using HadCM2 alone, which has the largest forced ensemble of greenhouse gas and sulphate aerosols, but the response pattern was

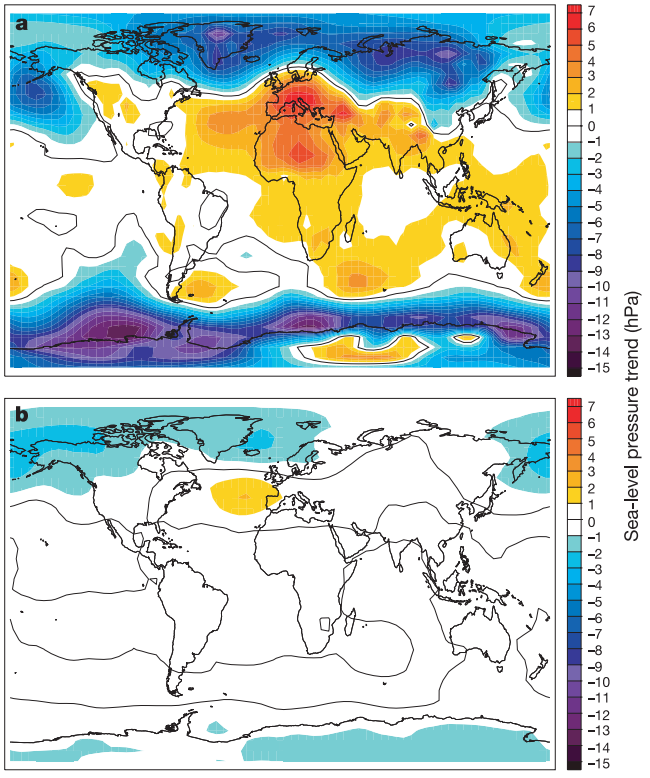

Figure 1 Observed and simulated sea-level pressure trends. The December–February sea-level pressure trends over the period 1948–1998 are shown **a**, for the NCEP reanalysis; and **b**, for the mean of the simulated response to greenhouse gas and sulphate aerosol changes from four climate models (CGCM1, CGCM2, HadCM2 and HadCM3). The pattern of trends is qualitatively similar in each case, but the simulated trends are much smaller in magnitude than those observed.

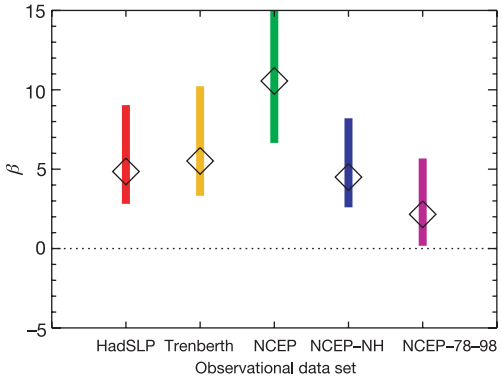

Figure 2 Regression coefficients, β, of observed sea-level pressure changes against changes simulated in response to greenhouse gas and sulphate aerosol increases. The first four bars show regression coefficients derived using a multi-model mean of simulated 1948–1998 sea-level pressure changes, and four observational data sets: HadSLP is a gridded data set of sea-level pressure measurements, defined only where observations are present[11]; Trenberth is a synthesis of analyses, only defined northward of 20° N[13]; NCEP is a global reanalysis[12]; and NCEP-NH is the NCEP reanalysis restricted to the Northern Hemisphere. The bar labelled NCEP-78-98 was derived using NCEP reanalysis data from 1978 to 1998 only. The 5–95% uncertainty ranges shown are derived from control variability and the squares represent best estimates.

not detected in every case when we used the other models individually.

Results based on the NCEP reanalysis were more consistent with those derived using the other data sets when only Northern Hemisphere data were used (Fig. 2), probably because of the effects of stratospheric ozone depletion and possible data problems over the Antarctic. To address the issue of possible discontinuities associated with the introduction of satellite data in the NCEP reanalysis around 1979, we repeated the analysis using only the final two decades of NCEP data (1978–1998), and found that the greenhouse gas and sulphate aerosol response was still detectable (Fig. 2).

Overall, we find that anthropogenic greenhouse gases and sulphate aerosols have had a detectable influence on sea-level pressure over the second half of the twentieth century: this represents evidence of human influence on climate independent of measurements of temperature change. We find that the observed pattern of December–February sea-level pressure trends is similar to that simulated in four climate models between 1948 and 1998, with decreasing sea-level pressure over the poles and North Pacific, and an increase over the subtropical North Atlantic. However, our results also indicate that these climate models may be substantially underpredicting this sea-level pressure response.

Circulation trends have had important regional impacts on climate: for example, the trend in the North Atlantic Oscillation has been associated with approximately 50% of the observed Eurasian winter warming over the past thirty years, over 60% of the rainfall increase in Scotland, and over 60% of the rainfall decrease in Spain over the same period[7]. It has also been linked to large changes in extreme events, for example over 70% of the decrease in extreme cold events in France[20]. On the basis of the results presented here, we conclude that such effects are probably underestimated in model simulations of both current and future climate change, although this does not invalidate the attribution of surface temperature trends to human influence[21]. However, if we are to make realistic predictions of regional climate change, it is important to reconcile this apparent discrepancy between models and observations. □

Received 10 September 2002; accepted 7 February 2003; doi:10.1038/nature01487.

1. Tett, S. F. B., Stott, P. A., Allen, M. R., Ingram, W. J. & Mitchell, J. F. B. Causes of twentieth-century temperature change near the Earth's surface. *Nature* **399,** 569–572 (1999).
2. Mitchell, J. F. B. *et al. Climate Change 2001. The Scientific Basis* Ch. 12 (Cambridge Univ. Press, Cambridge, UK, 2001).
3. Allen, M. R. *et al.* Quantifying anthropogenic influence on recent near-surface temperature change. *Surv. Geophys.* (in the press).
4. Tett, S. F. B., Mitchell, J. F. B., Parker, D. E. & Allen, M. R. Human influence on the atmospheric vertical temperature structure: Detection and observations. *Science* **274,** 1170–1173 (1996).
5. Barnett, T. P., Pierce, D. W. & Schnur, R. Detection of anthropogenic climate change in the world's oceans. *Science* **292,** 270–274 (2001).
6. Reichert, B. K. *et al.* Global ocean warming tied to anthropogenic forcing. *Geophys. Res. Lett.* DOI:10.1029/2001GL013954 (2002).
7. Thompson, D. W. J., Wallace, J. M. & Hegerl, G. C. Annular modes in the extratropical circulation. Part II: Trends. *J. Clim.* **13,** 1018–1036 (2000).
8. Shindell, D. T., Miller, R. L., Schmidt, G. A. & Pandolfo, L. Simulation of recent northern winter climate trends by greenhouse-gas forcing. *Nature* **399,** 452–455 (1999).
9. Fyfe, J. C., Boer, G. J. & Flato, G. M. The Arctic and Antarctic oscillations and their projected changes under global warming. *Geophys. Res. Lett.* **26,** 1601–1604 (1999).
10. Gillett, N. P. *et al.* How linear is the Arctic Oscillation response to greenhouse gases? *J. Geophys. Res.* DOI:10.1029/2001JD000589 (2002).
11. Basnett, T. A. & Parker, D. E. Development of the global mean sea-level pressure data set GMSLP2. *Clim. Res. Tech. Note* 79 (Hadley Centre, Met Office, Bracknell, UK, 1997).
12. Kalnay, E. *et al.* The NCEP/NCAR 40-year reanalysis project. *Bull. Am. Meteorol. Soc.* **77,** 437–471 (1996).
13. Trenberth, K. E. & Paolino, D. A. The Northern Hemisphere sea-level pressure data set: Trends, errors and discontinuities. *Mon. Weath. Rev.* **108,** 855–872 (1980).
14. Osborn, T. J. *et al.* Evaluation of the North Atlantic Oscillation as simulated by a coupled climate model. *Clim. Dyn.* **15,** 685–702 (1999).
15. Gillett, N. P., Graf, H. F. & Osborn, T. J. in *The North Atlantic Oscillation: Climatic Significance and Environmental Impact* Ch. 9 (American Geophysical Union, Washington DC, 2003).
16. Allen, M. R. & Tett, S. F. B. Checking for model consistency in optimal fingerprinting. *Clim. Dyn.* **15,** 419–434 (1999).
17. Lambert, S. J. & Boer, G. J. CMIP1 evaluation and intercomparison of coupled climate models. *Clim. Dyn.* **17,** 83–106 (2001).
18. Krishnamurti, T. N. *et al.* Improved weather and seasonal climate forecasts from multi-model superensemble. *Science* **285,** 1548–1550 (1999).
19. Gillett, N. P. *et al.* Detecting anthropogenic influence with a multi-model ensemble. *Geophys. Res. Lett.* DOI:10.1029/2002GL015836 (2002).
20. Thompson, D. W. J. & Wallace, J. M. Regional climate impacts of the Northern Hemisphere annular mode. *Science* **293,** 85–89 (2001).
21. Gillett, N. P. *et al.* Implications of changes in the Northern Hemisphere circulation for the detection of anthropogenic climate change. *Geophys. Res. Lett.* **27,** 993–996 (2000).

Acknowledgements We thank R. Allan and J. Arnott for supplying the HadSLP data set, and M. Allen for allowing us to use his optimal detection code. We thank NSERC and CFCAS for CLIVAR funding. A.J.W. is grateful for support from the Killam Foundation and the Canada Research Chair Program, and P.A.S. is grateful for support from the Department for Environment, Food and Rural Affairs.

Competing interests statement The authors declare that they have no competing financial interests.

Correspondence and requests for materials should be addressed to N.P.G. (e-mail: gillett@uvic.ca).

Enhanced mantle-to-crust rhenium transfer in undegassed arc magmas

Weidong Sun*, Vickie C. Bennett*, Stephen M. Eggins*, Vadim S. Kamenetsky† & Richard J. Arculus‡

** Research School of Earth Sciences, ‡ Department of Geology, The Australian National University, Canberra, ACT 0200, Australia*
† School of Earth Sciences and CODES SRC, University of Tasmania, Hobart, Tasmania 7001, Australia

Variations in the $^{187}Os/^{188}Os$ isotopic signature of mantle and mantle-derived rocks have been thought to provide a powerful chemical tracer of deep Earth structure. Many studies have inferred from such data that a long-lived, high-rhenium component exists in the deep mantle (^{187}Re is the parent isotope decaying to ^{187}Os, with a half-life of ~42 billion years), and that this reservoir probably consists of subducted oceanic crust[1–3]. The interpretation of these isotopic signatures is, however, dependent on accurate estimates of rhenium and osmium concentrations in all of the main geochemical reservoirs, and the crust has generally been considered to be a minor contributor to such global budgets. In contrast, we here present observations of high rhenium concentrations and low Yb/Re ratios in arc-type melt inclusions. These results indicate strong enrichment of rhenium in undegassed arc rocks, and consequently the continental crust, which results in a crustal estimate of ~2 p.p.b. rhenium, as compared to previous estimates of 0.4–0.2 p.p.b. (refs 4, 5). Previous determinations of rhenium in arc materials, which were largely measured on subaerially erupted samples, are likely to be in error owing to rhenium loss during degassing. High mantle-to-crust rhenium fluxes, as observed here, require a revaluation of geochemical models based on the ^{187}Re-^{187}Os decay system[1–3].

The major geochemical reservoirs of mid-ocean-ridge basalts (MORBs), depleted MORB mantle (DMM), continental crust (CC) and primitive mantle (PM) are not complementary in terms of Re contents or Re/lithophile-element ratios. For example, Re and the lithophile element Yb are similarly incompatible in the upper mantle during generation of MORB magma[1,6], which is best illustrated by the narrow range of Yb/Re (refs 1, 6; Fig. 1). This suggests that there is no major fractionation between Re and Yb during formation of MORB, and furthermore that the Yb/Re ratio

